Simulation of Electro-Impulse De-Icing Process Based on an Improved Ice Shedding Criterion

Yongjie Huang[1], Xian Yi[2,3(✉)], Qinglin Liu[2,3(✉)], Zhangsong Ni[1], Pan Pan[1], and Ying Zhang[1]

[1] Chengdu Fluid Dynamics Innovation Center, Chengdu 610010, China
[2] Key Laboratory of Icing and de-Icing Research, Aerodynamics Research, Mianyang 621000, China
yixian0105@126.com, caso@163.com
[3] State Key Laboratory of Aerodynamics, Aerodynamics Research, Mianyang 621000, China

Abstract. , The electro-impulse de-icing (EIDI) system has wide development potential in the field of aircraft green de-icing. For the design and optimization of EIDI, it is quite necessary to study ice shedding criterion and simulate the de-icing process. Based on experimental observations and theoretical analysis, an improved ice shedding criterion considering ice/skin debonding and ice fracture is proposed in this paper. Nonlinear transient three-dimensional finite element models combined with the ice shedding criterion are established to simulate the de-icing process. The simulation method is verified by experiments and literature comparison. Compared with the traditional ice shedding criterion, the improved ice shedding criterion and de-icing simulation results in this paper are more reasonable and accurate. A parametric study is performed to determine the influence of ice strength parameters on de-icing effectiveness. The results of the parametric study can provide guidance for the design of a compound EIDI system with higher de-icing efficiency.

Keywords: Electro-impulse De-Icing · Finite element method · Ice shedding criterion · Ice fracture · Ice/skin debonding

1 Introduction

Since the first successful test flight of the Wright Brothers in 1903, the development of aircraft has always been accompanied by flight accidents [1]. According to statistics, one of the main causes of flight accidents is meteorological conditions, among which icing conditions are a very dangerous problem that aircraft designers must pay attention to [2].

For the in-flight ice accretion problems, the current ice protection technology mainly includes passive anti-icing technology and active de-icing technology [3]. As a mechanical de-icing technology, electro-impulse de-icing (EIDI) potentially meets the basic ice protection requirements, such as low power requirements, light weight, simple structure, high reliability and high efficiency [4]. Compared with the traditional electric/gas-heat

Chinese Society of Aeronautics and Astronautics: CASTYSF 2022, LNEE 972, pp. 623–634, 2023.
https://doi.org/10.1007/978-981-19-7652-0_55

de-icing system, the EIDI has low infrared characteristics, which can be more suitable for stealth combat aircraft with strict requirements on infrared stealth performance. EIDI system has a wide range of application scenarios and application potential in the future.

The working principle of EIDI system is quite simple as shown in Fig. 1. The discharging of electric capacitors triggers the coils generating an electromagnetic field. The magnetic field then induces a mechanical impulsive loading, which causes the mechanical vibration of the aircraft skin and the ice shedding [5].

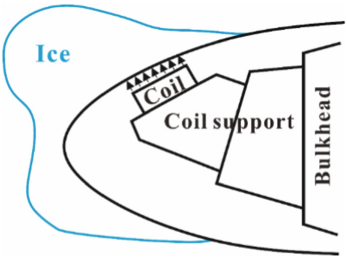

Fig. 1. Schematic diagram of EIDI system.

The earliest research on EIDI can be traced back to the 1930s [6]. The United States, the Soviet Union and the United Kingdom took the lead in carrying out the principal design and testing of EIDI system during this time. In the 1970s, the Soviet Union successfully applied the EIDI system to the Ilyshin series planes for the first time. However, due to various reasons, it was not widely promoted at that time [7]. Since the 1980s, the National Aeronautics and Space Administration (NASA) re-intensified the research of EIDI, and cooperated with Wichita State University and the Industry Consortium to carry out a series of icing wind tunnel experiments and flight tests [8]. Since 2010, Cox and Company of the United States successively developed Electro-Expulsive Separation System, Electro-Mechanical Expulsion De-icing System, Electro-Magnetic Expulsion De-icing System on the basis of EIDI system research, expanding and innovating EIDI technology [9].

The development of EIDI technology is inseparable from numerical simulation. Ice shedding process simulation and de-icing effectiveness prediction are of great significance to the engineering applications of EIDI system. The high accurate de-icing simulation model can help engineers quickly complete the design and analysis of the EIDI system. The finite element method (FEM) can discretize complex differential equations into linear equations to obtain stress and strain responses during EIDI process, and simulate the ice shedding based on damage mechanics.

Kandagal [10] and Palacios [11] believed that when the ice stress calculated by the dynamic model exceeded the bond strength between the ice layer and the aircraft skin, the ice layer would fall off. Khatkhate [12] used two-dimensional plane shell elements to model the aluminum skin and ice layer, and preliminarily predicted the ice shedding area on the skin surface under the impulsive load. The results indicated that shear stress between the skin and the ice layer was the main reason for the ice shedding. Considering the effect of interlayer normal tensile stress on ice shedding, Labeas [13] proposed an

ice shedding failure criterion based on the coupling of ice/skin interfacial shear stress and normal tensile stress, and established a three-dimensional progressive damage ice shedding finite element model for EIDI system. The numerical results showed that the ice shedding failure criterion could be used to predict the de-icing process of EIDI system, but the prediction accuracy was limited. Zhang [14] analyzed the contribution ratio of ice/skin interfacial shear stress and normal tensile stress to ice shedding, improved the ice shedding criterion and compared the influence of ice shedding criterion with different stress ratios on the ice shedding prediction. Based on the re-development of ANASYS, Li [7] compared the difference between the maximum stress criterion and the ice-skin interface shear-tension criterion in predicting the de-icing effectiveness of EIDI. Li found that one of the reasons for the limited accuracy of ice shedding prediction was that the traditional ice shedding model only considered the failure of the ice/skin interface.

Although a lot of work has been done on the numerical simulation of EIDI, few studies involve ice shedding failure criterion and damage analysis. There is still a lack of refined ice shedding failure criteria and progressive damage failure de-icing models. Besides, traditional ice shedding criteria for EIDI only consider the effect of interfacial stress on ice/skin debonding, ignoring the effect of ice fracture.

Aiming at the above problems, considering ice/skin debonding and ice fracture, an improved ice shedding failure criterion for EIDI was proposed in this study. 3D nonlinear transient dynamic finite element models were developed to simulate the de-icing process of EIDI system. The simulation results were compared with the experimental results and literature simulation results. A parametric study was performed to determine the influence of the ice strength parameters on de-icing effectiveness. The numerical method can be used in the engineering field to quickly evaluate the de-icing effectiveness of the EIDI system.

2 Numerical Simulation Method

2.1 Ice Shedding Mechanism and Ice Shedding Criterion

As mentioned in the previous literature [10–14], current ice shedding failure criteria for EIDI are basically based on debonding failure of the ice/skin interface. The effect of ice fracture on ice shedding is ignored. However, according to a simple de-icing experiment observation of EIDI system (as shown in Fig. 2a), under the impulsive load, ice shedding typically involves two failure modes: (a) ice/skin debonding and (b) ice fracture.

From the perspective of structural failure analysis, the ice-covered skin can be regarded as a composite structure, and the ice layer, the ice/skin interface and the skin are substructures respectively. The ice/skin debonding corresponds to the structural interlayer failure, and the brittle fracture of the ice layer corresponds to the intralayer failure (as shown in Fig. 2b). The damage to the substructures eventually leads to the overall ice shedding.

Under the impulsive load, the instantaneous stress state of the ice layer and its interface is very complex. On the one hand, there are interfacial shear stress and normal tensile stress at the ice/skin interface. As the interfacial stress exceeds the adhesion strength of the ice/skin interface, the ice layer and the skin will be debonded. On the

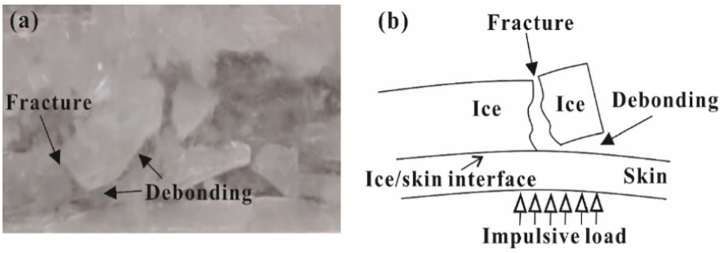

Fig. 2. Ice shedding mechanism for EIDI: **a** experimental phenomena, **b** failure analysis.

other hand, when the internal stress of the ice layer is large enough, it will promote the initiation of mode I crack in the ice layer, resulting in brittle fracture of ice.

Although it is difficult to capture the sequential relationship between ice/skin debonding and ice fracture in the EIDI experiment, it is obvious that the two failure modes can promote each other, and both eventually cause the ice shedding. Therefore, decomposing ice shedding into two failure modes: ice/skin debonding and brittle fracture of ice can more precisely and reasonably characterize the ice shedding phenomenon.

Based on the analysis of the ice shedding mechanism, an improved ice shedding criterion considering ice/skin debonding and ice fracture is proposed (as shown in Table 1), which is used for subsequent numerical simulation. When the stress state of the ice layer reaches the ice/skin debonding or ice fracture condition, it is determined that the ice layer falls off.

Table 1. Ice shedding criterion.

Ice shedding failure modes	Failure criterion
Ice/skin interface debonding	$f_{ID} = \begin{cases} \frac{\sigma_{\text{int}}}{\sigma_{\text{iu}}} + \left(\frac{\tau_{\text{int}}}{\tau_{\text{iu}}}\right)^2 \geq 1 \ (\sigma_{\text{int}} \geq 0) \\ \left(\frac{\tau_{\text{int}}}{\tau_{\text{iu}}}\right)^2 \geq 1 \ (\sigma_{\text{int}} 0) \end{cases}$ (1)
Ice fracture	$f_{BF} = \frac{\sigma_1}{\sigma_{\text{tu}}^{\text{I}}} \geq 1$ (2)

The ice/skin debonding is determined based on the Labeas criterion [13], which comprehensively considers the effects of interfacial normal stress and shear stress on interface debonding failure. σ_{int} and τ_{int} represent ice/skin interface normal tensile stress and shear stress respectively, while σ_{iu} and τ_{iu} represent ice/skin interface normal tensile strength and shear strength respectively. σ_{iu} is of 1.44 MPa and τ_{iu} is of 0.4 MPa [13].

The fracture failure of the ice layer is simplified into the brittle fracture model, and the first strength theory is used to determine the failure. σ_1 and σI tu represent maximum principal stress of the ice layer and ice tensile strength respectively, where σI tu is of 1.6 MPa [15].

2.2 Finite Element Model and Ice Shedding Failure Analysis Process

The de-icing model of EIDI system is built by using the structural parameters of the ice-covered aluminum skin plate given in literature [2] (as shown in Fig. 3a). The size of the aluminum plate is 420 mm × 420 mm and the thickness is 2 mm. Two sides of the aluminum plate are fixed while the other two sides are free. The ice layer is evenly covered on the aluminum plate, and the thickness of the ice layer is 3 mm. The elastic modulus of the aluminum plate is 71.5 GPa, the Poisson's ratio is 0.33, and the density is 2780 kg/m^3; the elastic modulus of the ice layer is 5.5 GPa, the Poisson's ratio is 0.3, and the density is 897 kg/m^3.

The meshing of the model is shown in Fig. 3b. The ice layer is set with one element along the thickness direction while the aluminum plate is set with four elements. The meshes are optimized in the central electromagnetic impulsive loading area, and the total number of elements is 33060. In order to improve the computation efficiency and avoid the occurrence of abnormal computation phenomena such as shear locking and hourglass, the 3D eight-node incompatible elements (C3D8I) and the continuum shell elements (SC8R) are used to mesh the ice layer and the aluminum plate respectively.

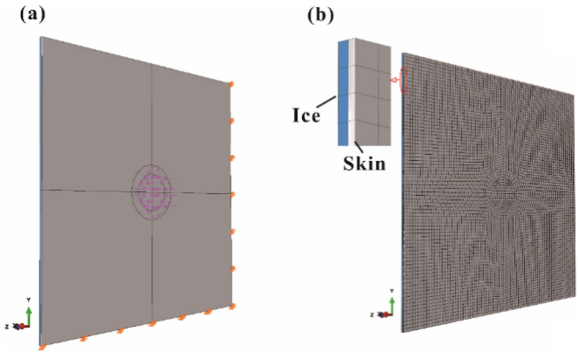

Fig. 3. Finite element model: **a** structure, **b** mesh.

The impulsive load generated by the EIDI system is applied to a 60 mm diameter area in the middle of the plate (as shown in Fig. 3a). Although the de-icing excitation acts on the skin for a very short time, the skin will still vibrate at its natural frequency after the driving force vanishes. As a result, the external load on the model can be described as shown in Fig. 4. The maximum impulse force is 130 N and the duration is 1 ms; the total de-icing process time is 80 ms.

De-icing simulation involves transient nonlinear dynamic numerical solution and ice shedding failure analysis. The whole process of EIDI de-icing simulation is shown in Fig. 5. t is the current time of the simulation process, and t_{max} is the total de-icing time. For each time increment Δt, the finite element dynamic equilibrium equation is established and solved, and the structural stress and strain responses are obtained. Afterwards, based on the improved ice shedding criterion, the ice shedding state is determined, and failed elements will be deleted.

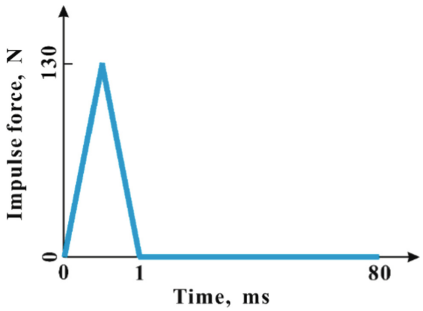

Fig. 4. The external load on the model.

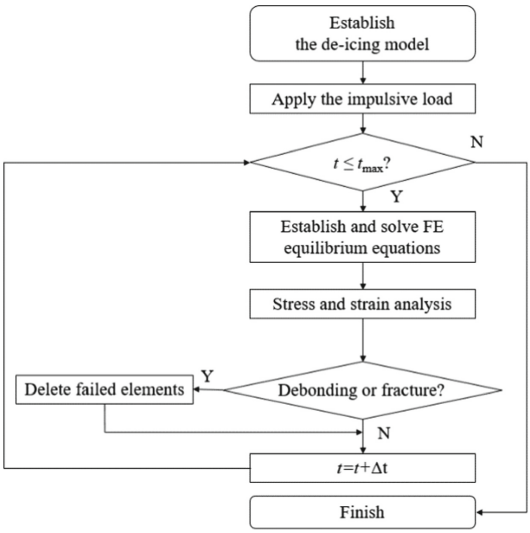

Fig. 5. Ice shedding failure analysis process.

The ABAQUS 2016/Explicit dynamics module is used to complete the transient dynamics solution of the finite element models, and the ABAQUS VUSDFLD is used for the failure analysis of ice shedding. The hardware platform for EIDI de-icing calculation is Intel Xeon Gold 6248R Server. The time to solve a single model is about 4 h.

3 Numerical Simulation Results and Analysis

3.1 Simulation Methodology Validation

To verify the accuracy of the de-icing model, the simulated results are compared with experimental and literature results (as shown in Fig. 6). The experimental conditions, structural geometry, material parameters and impulsive load are consistent with those in Sect. 2.2 for simulation models.

The de-icing experimental results [13] of the aluminum plate are shown in Fig. 6a. Due to the effect of impulsive loading induced by EIDI, most of the ice on the surface of the plate falls off, and only a small amount of ice is attached to the corner near the clamped boundary, forming an L-shaped region.

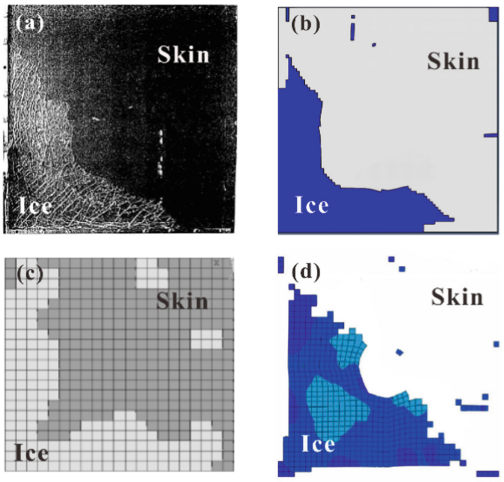

Fig. 6. Comparison of experimental and simulated results of de-icing process: **a** experimental result [13], **b** simulated result of this study, **c** simulated result of literature [13] and **d** simulated result of literature [14].

Figure 6b is the simulated results based on the improved ice shedding criterion proposed in this paper. Figure 6c and 6d are the simulated results of literature [13, 14], which are based on the traditional ice shedding criterion only considering ice/skin debonding failure.

From the comparison of the experimental and calculation results, it can be found that the predicted de-icing area and local characteristics of residual ice based on the improved ice shedding criterion are consistent with the de-icing experimental results, which proves the effectiveness of the simulation method. Moreover, the simulated results of the improved ice shedding criterion are more accurate than literature simulation results based on the traditional ice shedding criterion, indicating the improved ice shedding criterion are more reasonable.

3.2 Ice Shedding Failure Criterion Analysis

To analyze the effect of failure criteria on de-icing simulation, three kinds of ice shedding criteria were used for calculation: (a) ice shedding criterion considering both ice/skin debonding and ice fracture (as described in Eqs. (1) and (2)), (b) ice shedding criterion only considering ice/skin debonding (as described in Eq. (1)), (c) ice shedding criterion only considering ice fracture (as described in Eq. (2)). The simulated results of de-icing models corresponding to three ice shedding failure criteria are displayed in Fig. 7a, b, and c respectively.

The morphological characteristics of the residual ice calculated by ice shedding failure criteria (b) and (c) are quite different from the experimental result, which are also far inferior to the calculation result by ice shedding failure criterion (a). Moreover, the residual ice coverage areas predicted by ice shedding failure criteria (b) and (c) are much larger than the experimental result and the simulated result by ice shedding failure criterion (a), which also indicates that the failure criterion considering both ice/skin debonding and ice fracture is more reasonable than the failure criterion only considering ice/skin debonding or ice fracture.

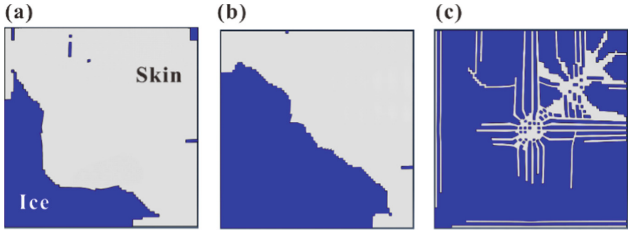

Fig. 7. Comparison of simulated results of ice shedding failure criteria: **a** criterion considering both ice/skin debonding and ice fracture, **b** criterion only considering ice/skin debonding, **c** criterion only considering ice fracture.

3.3 Parametric Study

Ice tensile strength, ice/skin interface normal tensile strength and ice/skin interface shear strength are three important strength parameters for the ice shedding criterion which affect both ice/skin debonding and ice fracture. In order to further clarify the influence of ice strength parameters on the de-icing process and provide a reference for the design of the EIDI system, a parameter analysis is carried out.

All investigated ice strength parameters for the de-icing simulation and their variations are presented in Table 2. The set of parameters corresponding to the benchmark is presented in the first column of the table. For each simulation, only one parameter changes, and the rest parameters keep the basic values. The variable range of the three strength parameters remains the same, which are 125%, 100%, and 75% of the basic values.

The de-icing effectiveness is quantitatively characterized by the de-icing rate, which is defined as the percentage of the de-icing area over the total plate area. The higher the de-icing rate, the better the de-icing effectiveness.

Ice tensile strength. Ice tensile strength is a physical parameter of the ice layer itself, which is affected by many factors such as the diameter of the water droplet, the air flow velocity, temperature, and ambient humidity. Ice tensile strength measured under different experimental conditions is quite different and it has a high dispersion.

The range of ice tensile strength investigated in this paper is 2.0 MPa (125%), 1.6 MPa (100%) and 1.2 MPa (75%). The simulated de-icing results of EIDI system are shown in Fig. 8a, b, and c, respectively. It can be seen that with the decrease of the ice tensile

Table 2. Strength parameters investigated and their variations.

Parameter	Basic set of parameters		
Ice tensile strength	1.6 MPa (100%)	2.0 MPa (125%)	1.2 MPa (75%)
Ice/skin interface normal tensile strength	1.44 MPa (100%)	1.8 MPa (125%)	1.08 MPa (75%)
Ice/skin interface shear strength	0.4 MPa (100%)	0.5 MPa (125%)	0.3 MPa (75%)

strength, the calculated de-icing rate gradually increases, indicating that the ice tensile strength is inversely proportional to the de-icing effectiveness within a certain range. Lower ice tensile strength is conducive to the ice shedding, which also reflects the rationality and necessity of considering ice fracture in the ice shedding failure criterion.

Fig. 8. The influence of ice tensile strength on de-icing rate.

Ice/skin interface normal tensile strength. The adhesion strength of the ice/skin interface is not only related to the physical parameters of the ice layer, but also affected by the properties of the skin material, the coefficient of friction and the mesoscopic geometric characteristics of the interface. There are many experimental studies on the ice/skin interface shear strength, but few studies on the ice/skin interface normal tensile strength. The range of ice/skin interface normal tensile strength investigated in this paper is 1.8 MPa (125%), 1.44 MPa (100%) and 1.08 MPa (75%). The predicted de-icing results of EIDI system are shown in Fig. 9a, b, and c, respectively.

The results show that the de-icing rate gradually increases with the decrease of the ice/skin interface normal tensile strength. However, the increase of the de-icing rate is limited and the residual ice morphology characteristics does not change significantly. It indicates that under the same strength ratio range (75% ~ 125%), the effect of ice/skin interface normal tensile strength on ice shedding is less than that of ice tensile strength.

Ice-skin interface shear strength. The range of ice/skin interface shear strength investigated in this paper is 0.5 MPa (125%), 0.4 MPa (100%), and 0.3 MPa (75%). The predicted de-icing results of EIDI system are shown in Fig. 10a, b, and c, respectively.

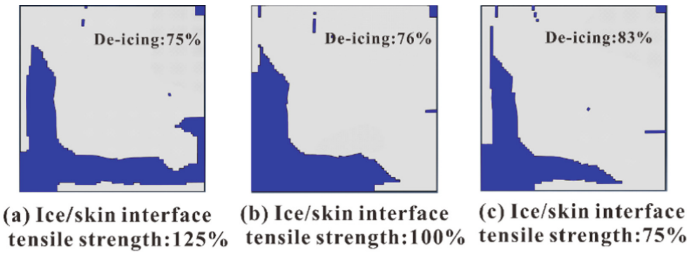

Fig. 9. The influence of ice/skin interface normal tensile strength on de-icing rate.

The simulated results show that the ice/skin interface shear strength has a significant effect on ice shedding. With the decrease of ice/skin interface shear strength, the de-icing rate increases from 47% to 98%. Moreover, compared with the ice tensile strength and ice/skin interface normal tensile strength, under the same conditions, the ice/skin interface shear strength has a more prominent influence on the de-icing process.

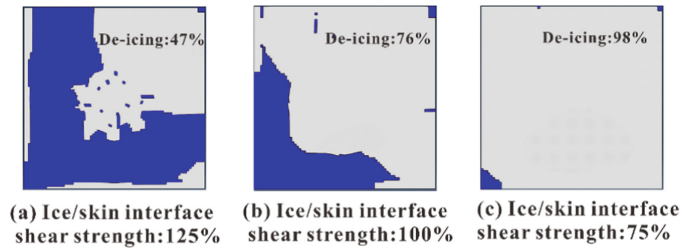

Fig. 10. The influence of ice/skin interface shear strength on de-icing rate.

Therefore, in the design or simulation of the anti-icing system, it is necessary to pay more attention to the ice/skin interface shear strength. On the one hand, the accurate acquisition of the ice/skin interface shear strength value is helpful to improve the numerical simulation accuracy; on the other hand, through surface treatment technology, artificially reducing the ice/skin interface shear strength can significantly increase the effectiveness of EIDI system.

Furthermore, the comprehensive use of EIDI and surface materials with low ice adhesion strength (e.g. superhydrophobic materials) to construct a new compound EIDI system has a potential to further improve the anti-icing efficiency and reduce energy consumption, which is worthy of further research in related fields.

4 Conclusions

(1) Based on the experimental observation and theoretical analysis, the ice shedding process of EIDI can be refined and decomposed into two failure modes: ice/skin debonding and ice fracture.

(2) An improved ice shedding criterion considering ice/skin debonding and ice fracture is proposed in this paper. Compared with the experimental and simulated results in the literature, the de-icing simulation results based on the improved ice shedding criterion are more accurate and reasonable than traditional criteria which only consider ice/skin debonding failure.
(3) The de-icing rate of EIDI system increases with the decrease of ice tensile strength, ice/skin interface normal tensile strength and ice/skin interface shear strength. Compared with the other strength parameters, ice/skin interface shear strength has the most significant effect on the de-icing effectiveness of EIDI.
(4) A new compound de-icing system based on EIDI system and surface materials with low ice adhesion strength has a potential to further improve the de-icing efficiency and reduce energy consumption.

Acknowledgements. The authors would like to thank the National Natural Science Foundation of China (No.12132019) for their support in this research.

References

1. Tianxiang, Z.: Statistical analysis of aircraft accidents and their causes. Aviat. Stand. Qual. **12**(6), 37–43 (1998). (in Chinese)
2. Wei, Y., Xu, H., Xue, Y., Duan, X.,: Quantitative assessment and visualization of flight risk induced by coupled multi-factor under icing conditions. Chin. J. Aeronaut. **8**(173), 52–67 (2020)
3. Goraj, Z.: An overview of the de-icing and anti-icing technologies with prospects for the future. In: 24th Congress of International Council of the Aeronautical Sciences, pp. 34–42. Yokohama, Japan (2004)
4. Potapczuk, M.G.: Aircraft icing research at NASA Glenn research center. J. Aerosp. Eng. **26**, 260–276 (2013)
5. Fan, G., Shinan, C.: Design test of electro- impulse de-icing system of an aircraft. In: 2nd International Conference on Artificial Intelligence, Management Science and Electronic Commerce (AIMSEC), Zhengzhou, China, (2011)
6. Levin, I.: A: USSR electric impulse de-icing system design. Aircr. Eng. Aerosp. Technol. **44**(7), 7–10 (1972)
7. Li, Q., Zhu, C., Tian, B.: Numerical simulation and experimental verification of the electro-impulse de-icing system. In: 53rd AIAA/ASME/ASCE/AHS/ASC Structures, Structural Dynamics and Materials Conference, Honolulu, Hawaii (2012)
8. Zumwalt, G., Friedberg, R.: Designing an electro-impulse de-icing system. AIAA J. 1–9 (1986)
9. Al-Khalil, K.: Thermo-mechanical expulsive de-icing system – TMEDS. In: 45th AIAA Aerospace Sciences Meeting and Exhibit, Reno, USA (2007)
10. Kandagal, B.: Piezo-actuated vibratory de-icing of a flat plate. In: 46th AIAA/ASME/ASCE/AHS/ASC Structures, Structural Dynamics and Materials Conference, Austin, USA (2005)
11. Palacios, J.L.: Design, fabrication, and testing of an ultrasonic de-icing system for helicopter rotor blades. PhD thesis, The Pennsylvania State University (2008)

12. Khatkhate, A.A., Scavuzzo, R.J., Chu, M.L.: A finite element study of the EIDI system. AIAA J. (1988)
13. Labeas, G.N., Diamantakos, I.D., Sunaric, M.M.: Simulation of the electro-impulse de-icing process of aircraft wings. J. Aircr. **43**(6), 1876–1885 (2006)
14. Yongjie, Z., Wenjun, D., Bintuan, W.: Study on de-icing criterion of electro-impulse de-icing simulation. Comput. Eng. Appl. **48**(3), 232–233 (2012). (in Chinese)
15. Reich, A.: Ice property/structure variations across the glaze/rime transition. In: 30th Aerospace Sciences Meeting and Exhibit, Reno, USA (1992)